Applied Nanoscience (2023) 13:1919–1937
https://doi.org/10.1007/s13204-021-01881-w

ORIGINAL ARTICLE

Anticancer, anti-biofilm and antimicrobial activity of fucoidan-loaded zeolitic imidazole framework fabricated by one-pot synthesis method

Prabhu Raju[1] · **Suganthy Natarajan**[1]

Received: 6 January 2021 / Accepted: 8 May 2021 / Published online: 17 May 2021

Abstract

Biocompatible drug delivery system with precise and sustained release is necessary for biomedical applications. Zeolitic imidazole frameworks (ZIF-L), an emerging porous material, have been widely reported as efficient platform for the drug delivery. The present study focuses on one-pot organic solvent-free synthesis of fucoidan-loaded ZIF-L (FU@ZIF-L) and assess its biomedical applications. Antimicrobial, anticancer efficiency and biocompatibility of FU@ZIF-L was systematically investigated. Formation of FU@ZIF-L was confirmed by UV–Visible spectroscopy, while XRD analysis revealed presence of two-dimensional flaky crystalline structures, which was substantiated by TEM analysis. DLS analysis showed homogenously distributed crystals with particle size of 78 nm suitable for cellular intake. Results revealed that FU@ZIF-L exhibited potent antimicrobial activity against *Bacillus subtilis, Staphylococcus aureus, Klebsiella pneumonia* and *Escherichia coli.* In addition, FU@ZIF-L was observed to be more efficient in piercing and disturbing the biofilm architecture of methicillin-resistant *Staphylococcus aureus* and *E. coli*. Furthermore, FU@ZIF-L exhibited cytotoxic effect against A549 cells with IC_{50} value of 38.5 ± 2.34 µg/ml. ROS-mediated nuclear damage might be the reason for its anticancer potential. Brine shrimp lethality assay confirmed the biocompatible nature of FU@ZIF-L. To conclude, ZIF-L acts as effective drug delivery system for fucoidan enhancing its biomedical applications.

Keywords Zeolitic imidazole frameworks (ZIF-L) · Anti-biofilm · Antimicrobial · *Artemia salina* · A549 cells · Fucoidan

Introduction

Nanomaterials due to its unique physiochemical properties, overcomes the limitations of drug encapsulation or surface adherence facilitating cellular interaction, targeted delivery to desired site with slow and sustained release of drug molecules (Sun et al. 2012; He et al. 2015). Major limitation of chemotherapy is non-specific delivery of drugs affecting the healthy tissues, which signifies the need for suitable drug delivery system (AbdelHamid et al. 2017; Yu et al. 2015; Zhang et al. 2017). Advancement in nanotechnology has increased the interest of researchers towards, organic and inorganic nanomaterial for biomedical research (McNamara and Tofail 2017). Metal organic frameworks (MOFs) have received tremendous interest worldwide as drug designing analogue of anticancer drug delivery systems (Biswal et al. 2013; Zheng et al. 2016). The advantageous properties of MOFs like large surface area, high drug loading capacity, thermal stability, porosity and pseudo-bonding responsible for biodegradability, enhances the biological potential of drugs and material stability (Lee et al. 2015; Wang et al. 2015). MOF-based drug delivery systems are nontoxic to healthy cells and they release targeted molecules only to cancer cells (Adhikari et al. 2015; James and Lin 2016). Zeolitic imidazole framework (ZIF-L) represents a new class of nontoxic biodegradable metal organic framework formed by acidic zinc ions and basic imidazole ligands. ZIF-L-based drug delivery systems have been considered as an alternative cargo for toxic organic and inorganic nanoparticles in the field of biomedicine (Chowdhuri et al. 2016; Tiwari et al. 2017; Zhang et al. 2017). Zinc ions present in ZIF-L is an essential micronutrient, which plays vital role in immune response (Kambe et al. 2015), while the ligand imidazole group of ZIF-L acts as integral part of biomolecules like histidine and porphyrin ring of hemoglobin and myoglobin (Narasimhan et al. 2011). The proposed drug fucoidan, a sulfated polysaccharide isolated from brown sea weeds have

✉ Suganthy Natarajan
suganthy.n@gmail.com; suganthyn@alagappauniversity.ac.in

[1] Department of Nanoscience and Technology, Alagappa University, Karaikudi, Tamilnadu 630002, India

been reported for its anticancer, anticoagulant, antibacterial, apoptotic, angiogenic and anti-inflammatory activities (Cho et al. 2015; Ikeguchi et al. 2015; Zhang et al. 2015; Li et al. 2016). Furthermore, the functional groups such as sulfate, hydroxyl and carboxylic groups present in fucoidan also exhibit absorption and chemical conjugation properties (Jun et al. 2018; Khan et al. 2019; Ashayerizadeh et al. 2020). Despite of its wide pharmacological efficiency, poor solubility and instability of fucoidan at physiological pH, demands a suitable drug delivery system. Hence, the present study focused on encapsulation of fucoidan drug moiety within ZIF-L to enhance the anticancer potential of fucoidan by improving its bioavailability, solubility and delivery of drug to the target site. In the present study, fucoidan encapsulated ZIF-L nanocomposite was synthesized by solvent-free one-pot synthesis method and assessed for its antibiofilm and antimicrobial activities. The ultimate focus of the research was to eradicate human pathogens and lung cancer cells using sulfated polysaccharide fucoidan encapsulated ZIF-L nanocomposite based on the pH-responsive drug release mechanism.

Materials and methods

Chemicals used

Zinc nitrate hexahydrate ($Zn(NO_3)_2.6H_2O \geq 99\%$), 2-methyl imidazole, fetal bovine serum, penicillin, streptomycin, DMEM high-glucose medium were purchased from Himedia Laboratories Pvt. Ltd, India. Fucoidan from *Fucus vesiculosus* ($C_{15}H_{14}O_6.xH_2O \geq 98\%$), and all the fluorescence stains used for cell culture were purchased from Sigma Aldrich, USA. Human lung cancer cell line A549 was obtained from National Center for Cell Science (NCCS).

Fabrication of FU@ZIF-L nanocomposite

FU@ZIF-L was fabricated by simple one-pot synthesis method. Zn $(NO_3)_2$ (13.44 mM) and 2-Methyl imidazole (146 mM) in the ratio 1:3 was used for synthesis of ZIF-L based on methodology of Zheng et al. (2016) with some modifications. Briefly, Zn $(NO_3)_2$ in aqueous medium (13.44 mM) was subjected to vigorous stirring for half an hour at room temperature and then 2-methyl imdiazole (146 mM) was added drop wise. Reaction mixture was subjected to stirring (30 min) until white colloid appears which illustrates the formation of leaf-like zeolitic imidazole frameworks (ZIF-L). Finally, 20 ml of fucoidan (1 mg/ml) solution was added slowly to the ZIF colloid under magnetic agitation which was continued for another 1 h. The reaction mixture was centrifuged at 10,000 rpm for 30 min and the precipitate was washed thrice with double distilled water followed by drying at 60 °C for 6 h.

Drug loading efficiency

The quantification of fucoidan loading in ZIF-L nanoparticles was measured by the absorbance of fucoidan at 260 nm in UV–Vis spectroscopy. Total content of fucoidan in ZIF-L nanoparticles was determined by decomposition of FU@ZIF-L nanocomposite in HCl aqueous solution. The quantification was done with the calibration curve of fucoidan. The amount of drug loaded was calculated as mentioned below

$$\text{Drug loading capacity} = \frac{\text{Amount of drug loaded}}{\text{Total amount of drug loaded NPs}} \times 100,$$

where the drug loading capacity (DLC) of FU@ZIF-L was calculated to be 20.06%.

Characterization of fucoidan-loaded ZIF-L nanocomposite (FU@ZIF-L)

Crystalline nature and size of synthesized ZIF-L and FU@ZIF-L was analyzed by powder X-ray diffraction spectroscopy (PRO PANALYTICAL, model no.PW3040/60, X'PERT software). Surface plasma resonance of FU@ZIF-L nanocomposite was evaluated by UV–Visible spectrophotometer (Varian model Cary 5000 scan) and the characteristic absorption spectrum was measured by wavelength scan in the range 200–800 nm. Functional group of FU@ZIF-L was analyzed by FTIR spectral analysis in wavenmber ranging from 4000 to 400 cm^{-1} with resolution of 4 cm^{-1} (Bruker Optik GmbH, Model No. Tensor 27, Germany). Surface morphological features of nanocomposite were assessed using Field Emission Scanning Electron Microscopy (FESEM) (Carl Zeiss, Germany). The crystal morphology and size of FU@ZIF-L was studied by using High resolution transmission Electron Microscopy (HR-TEM) (FEI, Netherland, model no. Tecnai, G2 F20). Particle size of synthesized FU@ZIF-L nanoccomposite was analyzed through dynamic light scattering (DLS) analysis (Micrometrics, Nano Plus).

Anticancer studies

Cytotoxic effect of FU@ZIF-L nanocomposite

The inhibitory concentration of FU@ZIF-L nanocomposite against A549 cancer cells were analyzed by MTT [3-(4, 5-dimethylthiazol-2-yl)-2, 5-diphenyltetrazolium bromide] assay in accordance to the methodology of (Deepikaet al. 2019). A549 cells were allowed to grow overnight followed by treatment with various dose of FU@ZIF-L

nanocomposite (20–100 µg/mL). After 24 h exposure to FU@ZIF-L nanocomposite, the cells incubated with MTT (1 mM) for 4 h at 37 °C, followed by the dissolution of blue-colored formazan with DMSO and the absorbance was measured 570 nm in multi-plate reader (Molecular Device Spectramax M3, equipped with Softmax Pro V5 5.4.1 software). Percentage of cell viability was calculated.

Assessment of ROS generation

Intracellular ROS level was analyzed using DCFH-DA (2'-7'dichlorofluorescin diacetate) fluorescence dye. Overnight adhered cells were exposed to FU@ZIF-L (IC_{50} 38.5 ± 2.34 µg/ml) for 24 h. Treated cells was incubated at 37 °C with DCFH-DA (50 µl) for half an hour and the intensity of fluorescence was measured using fluorescence spectrophotometer (Cary Eclipse, Varian) with excitation wavelength of 480 nm and emission wavelength of 530 nm, respectively. Fluorescence microscopic images were taken using fluorescent microscope (Carl Zeiss Axio Observer Z1, Germany).

Hoechst staining

The nuclear damage induced by FU@ZIF-L nanocomposite was analyzed by using Hoechst dye. FU@ZIF-L nanocomposite-treated cells were exposed to Hoechst 33258 staining (1 mg/ml) for 15 min. Excess stain was removed by PBS wash and the intensity of fluorescence was analyzed at excitation/emission wavelength of 350/460 nm using spectrofluorimeter. Fluorescent microscopic images of the cells were captured in fluorescent microscopy.

Anti-biofilm potential of FU@ZIF-Lnanocomposite

Biofilm inhibition potential of FU@ZIF-L nanocomposite against MRSA and *E.coli* were analyzed in accordance to protocol of Ishwarya et al. (2018). MRSA and *E. coli* (O/N) culture was diluted to 10^8 CFU/ml using TSB broth with 0.5% glucose followed by treatment with different doses of FU@ZIF-L nanocomposite (20–100 µg/ml), for 48 h at 37ºC. Free floating planktonic bacteria were removed by PBS followed by treatment with crystal violet (0.4%). Slides were subjected to distilled water wash to remove excess stain, followed by treatment with glacial acetic acid (10%) for 10 min, and the absorbance was analyzed at 570 nm.

Microscopic visualization of biofilm morphology

Changes in the biofilm architecture of FU@ZIF-L nanocomposite-treated groups were analyzed by light microscopic analysis. FU@ZIF-L-treated biofilm formed glass slides were stained with crystal violet (0.2%) followed by distilled water wash to remove excess stain and the biofilm formed was visualized under light microscope (Lawrence & Mayo) at 40 × magnification.

Antibacterial activity of FU@ZIF-L nanocomposite

Antimicrobial activity of FU@ZIF-L nanocomposite was assessed against *B. subtilis* (MTCC 441), *S. aureus* (MTCC 96), *E. coli* (MTCC 40) and *K. pneumonia* (MTCC 8911) by agar well-diffusion method. Overnight bacterial culture (0.1%) was swabbed uniformly over the surface of Muller Hinton Agar. Different doses of ZIF-L and FU@ZIF-L nanocomposite (25–100 µg/mL) were loaded into wells and subjected to incubation at 37 °C for 12 h. Results were expressed as diameter of clear zone of inhibition in mm.

Minimum inhibitory concentration (MIC) of FU@ZIF-L against *S. aureus* and *K. pneumonia* was evaluated by microdilution method in accordance to methodology of CLSI (2006). Briefly, bacterial cultures (10^6 CFU/mL) were exposed to different dose of FU@ZIF-L (20–2560 µg/mL) overnight at 37 °C and the absorbance was recorded at 600 nm using multi-plate reader. Experiments were carried out in triplicates. To assess the minimum bactericidal concentration (MBC), aliquots of tube with no detectable bacterial growth were plated in MHA plates and incubated overnight at 37 °C (Shanholtzer et al. 1984). MBC is defined as the least dose of nanocomposite at which no live cells were observed.

Collection of *Artemia salina* cysts

Artemia salina is the most widely used in vivo model system for assessment of ecotoxicity and toxicity of engineered nanomaterials due to its low cost, convenience, rapidity in assessment when compared to animal model system. Freeze dried *Artemia salina* cysts were commercially purchased from VGP marine kingdom Chennai. Cleaned dried cyst (0.5 g) was allowed to incubate in artificial seawater at 30 ± 1 °C under constant illumination and aeration, which facilitated hatching of cyst within 24 h. The freshly hatched nauplii were transferred in to fresh seawater for further experiment.

Brine shrimp lethality assay

Cytotoxic effects of FU@ZIF-L nanocomposite was assessed by brine shrimp lethality assay using *Artermia salina* as model system (Rajabi et al. 2015). Freshly hatched *Artemia salina* nauplii (no. 25) were placed in each well and subjected to treatment with different concentrations of FU@ZIF-L (25–150 µg/ml) in sea water for 48 h. Number of dead and viable shrimp was counted using magnifying glass. *Artemia salina* nauplii in sea water without FU@ZIF-L was

used as negative control. Live and death nauplii was analyzed using magnification lenses and $LC_{50}$was calculated. Mortality rate of *Artemia salina* nauplii was calculated by comparing number of survivors in treated and control using Abbott's formula

$$\% \text{ of lethality} = \frac{\text{Nt - Nc}}{\text{Nc}} X100,$$

where Nt and Nc is the number of surviving *A. salina naupli* in treated group and control group.

In vitro drug release mechanism of FU@ZIF-L nanocomposite

The in vitro pH-responsive drug release mechanism of fabricated FU@ZIF-L nanocomposite was assessed at different pH (5, 6 and 7.4). Prior to drug release kinetics, the calibration graph for fucoidan (drug) was plotted by measuring the absorbance at 260 nm at which the fucoidan would exhibit maximum absorption. Approximately, 50 mg of FU@ZIF-L nanocomposite was suspended in 50 mL of PBS buffer and subjected to low speed (150 rpm) magnetic stirring at 37 °C. Aliquots were taken from the mother solution (FU@ZIF-L nanocomposite), subjected to centrifugation and the volume of aliquots taken is replaced with fresh PBS solution. The amount of drug released was calculated by measuring absorbance at 260 nm using the calibration curve and the percentage of drug release was calculated.

In vitro assessment of cytotoxic and hemolytic activity of FU@ZIF-L nanocomposite

The cytotoxic effect of FU@ZIF-L nanocomposite in human peripheral blood mononuclear cells (PBMC) was evaluated by trypan blue dye exclusion method based on the cell membrane integrity (Sivamaruthi et al. 2019). Isolated PBMC cells were exposed to different doses of FU@ZIF-L (100–500 µg/ml) at 37 °C for 24 h. Cells were treated with trypan blue (10 µg/mL) dye for 10 min and the percentage of viable cells were calculated as mentioned below. Hydrogen peroxide (250 µM) was used as positive control

$$\text{Percentage of cell viability} = \frac{\text{Viable cell count}}{\text{Total number of cells}} \times 100.$$

Blood compatibility of FU@ZIF-L nanocomposite was evaluated by hemolytic assay in accordance to the method of Dobrovoiskaia et al. (2008). To isolate erythrocytes the blood samples collected from healthy volunteers were diluted in the ratio 1:2 with PBS and centrifuged at 3000 rpm for 10 min. Isolated RBC was diluted with PBS and the around 200 µl of blood sample was treated with different dose of FU@ZIF-L (100–500 µg/ml) for 1 h at physiological temperature. Triton × 100 and PBS-treated cells were used as positive and negative control. Supernatant (100 µl) of all treated samples were collected and the absorbance was measured at 577 nm. Percentage of hemolysis was measured as represented below

$$\% \text{ of hemolysis} = \frac{\text{Absorbance of Test - Absorbance of NC}}{\text{Absorbance of PC - Absorbance of NC}} \times 100.$$

Statistical analysis

Probit analysis software was used to calculate IC_{50}, LD_{50} and LD_{90} value and comparison of control and treated groups were carried out using one-way analysis of variance (ANOVA) using SPSS 17.0 software. $*p < 0.05$ indicates significance.

Results and discussion

Powder XRD and UV–Vis analysis

The crystalline nature of the fabricated ZIF-L and FU@ZIF-L nanocomposite was studied by Powder XRD analysis. Figure 1A reveals that, the ZIF-L alone showed sharp diffraction peaks at 14.61 º, 15.73 º, 16.53 º, 21.12 º, 25.71 º, 27.41 º, 29.61 º, 30.46 º, 35.61 º, 37.27 º, 41.19 º and 43.21 º corresponding to (100), (002), (101), (102), (110), (103), (200), (201), (104), (203), (114) and (104) Braggs reflection planes. Characteristic diffraction peaks at 2θ values and planes represent that two-dimensional flaky crystal structured ZIF-L in according to JCPDS No. 01-1136 and report of Chen et al. (2013). The PXRD pattern of FU@ZIF-L nanocomposite exhibit some additional diffraction peaks other than observed in ZIF-L revealing uniform encapsulation of fucoidan with in ZIF-L forming nanocomposite. PXRD spectra of FU@ZIF-L nanocomposite matched well with JCPDS: 38-1922 indicating rhombohedral crystal structure. The crystalline size of ZIF-L and FU@ZIF-L nanocomposite was measured by Scherer's formula to be around 53.18 and 46.25 nm, respectively. The additional peaks and crystalline size reduction of FU@ZIF-L nanocomposite indicated that the encapsulation of fucoidan into ZIF-L frameworks disturbed the crystalline nature of ZIF-L nanoparticles.

The characteristic absorption spectra of FU@ZIF-L nanocomposite showed peak at 212 nm, respectively (Fig. 1B). Fucoidan and ZIF-L alone showed absorption peaks at 260 and 220 nm, respectively, as reported by Prabhu et al. (2020). Shift in the absorption peak of FU@ZIF-L nanocomposite might be due to encapsulation of fucoidan in ZIF-L. Band gap energy of ZIF-L and FU@ZIF-L nanocomposite was calculated to be 5.63 eV and 5.84 eV, respectively.

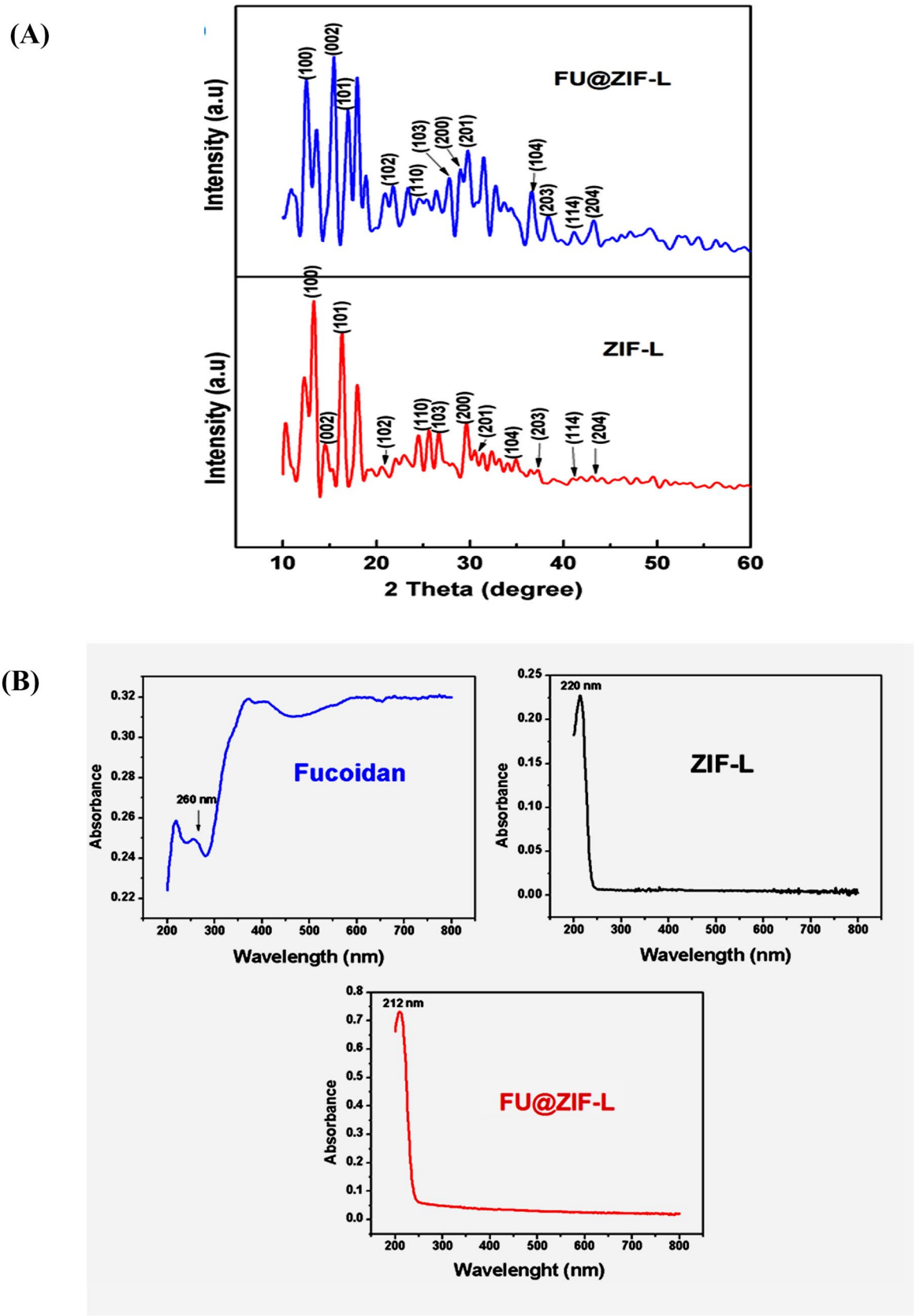

Fig. 1 (**A**) Powder XRD analysis of ZIF-L (red) and FU@ZIF-L (blue); (**B**) UV–Vis spectra of ZIF-L (black), FU@ZIF-L (red) and fucoidan (blue)

FTIR analysis

The identification of functional groups of synthesized ZIF-L and FU@ZIF-L nanocomposite were studied using FTIR spectroscopy technique. The FTIR spectra of FU@ZIF-L nanocomposite and ZIF-L alone were similar except additional peaks (Fig. 2) in nanocomposite, which might be due to presence of sulphated polysaccharide fucoidan. The sharp peaks at around 423 cm^{-1}, 684 cm^{-1} represented the stretching vibration of Zn-N bonds formed between zinc and imidazole binder during the formation of ZIF-L and FU@ZIF-L nanocomposite. Intense peaks at 998 cm^{-1} and 1154 cm^{-1} confirmed the C-N stretching vibration of imidazole linkers in ZIF-L and FU@ZIF-L. The IR spectral bands at around 1595 cm^{-1} and 1623 cm^{-1} corresponds to C = O stretching vibration. The less intense peak at around 585 cm^{-1} and 843 cm^{-1} represents the C-O-S stretching vibration of sulfur groups in fucoidan and FU@ZIF-L nanocomposite. Small peak at around 2921 cm^{-1} represents C-H vibration of imidazole linker from ZIF-L frameworks. This peak was shifted to 2934 cm^{-1} in FU@ZIF-L nanocomposite due to the incorporation of fucoidan molecules.

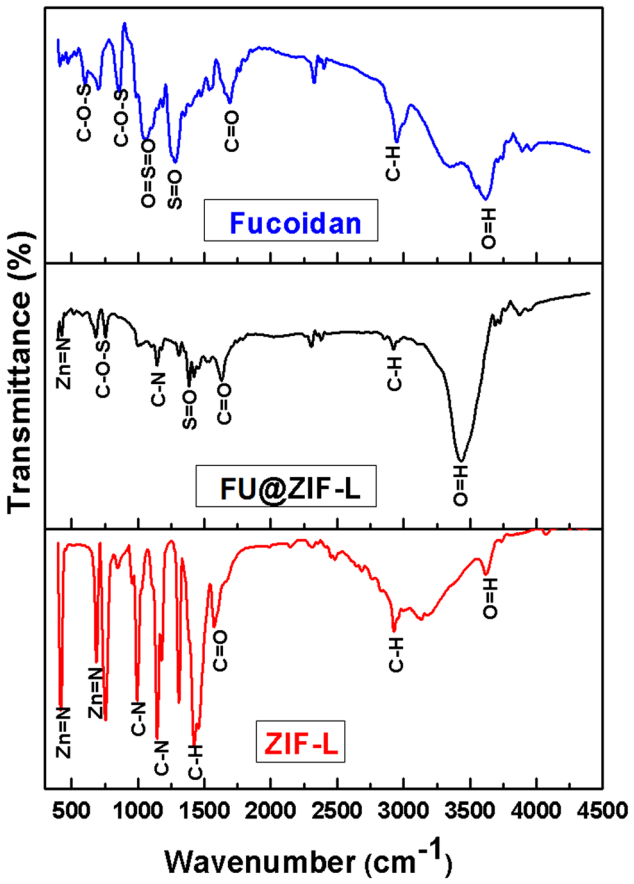

Fig. 2 FTIR spectra of ZIF-L (red), FU@ZIF-L (black) and fucoidan (blue)

SEM and EDX analysis

Morphology and elemental composition of synthesized nanocomposite was assessed through SEM and EDX analysis. SEM image of bare ZIF-L reveals the presence of uniform thin layer of nanoflakes with leaf-like 2D crystalline structure (Fig. 3A) as reported by Khana et al. (2018). SEM image of FU@ZIF-L nanocomposite revealed presence of nanoscale agglomerated sphere-like crystals (Fig. 3C). In one-pot synthesis method, simultaneous addition of fucoidan to ZIF-L disturbed the 2-D crystalline growth and uniformity of ZIF-L thereby reducing size of crystals. EDX spectral analysis of ZIF-L and FU@ZIF-L nanocomposite (Fig. 3B, D) depicted that no other elemental impurities were present in the prepared nanocomposite. The atomic percentage of elements in FU@ZIF-L nanocomposite differs on fucoidan encapsulation. Total weight percentage zinc in ZIF-L and FU@ZIF-L nanocomposite are 35.17 and 32.89%, respectively. Reduction in the total weight percentage of Zn^{2+} in FU@ZIF-L nanocomposite might be due to replacement of zinc ions by fucoidan molecule during the formation of FU@ZIF-L nanocomposite.

TEM and DLS analysis

The HR-TEM images of synthesized ZIF-L and FU@ZIF-L nanocomposite are shown in Fig. 4A. TEM images of ZIF-L exhibited [Fig. 4A (a, b)] two-dimensional flakes, while FU@ZIF-L nanocomposite [Fig. 4A (c, d)] showed agglomerated spheres. Average particle size of FU@ZIF-L nanocomposite was calculated as 37.8 nm. Figure 4B reveals the hydrodynamic diameter of synthesized nanocomposite in solution. Average particle size was observed to be 78.3 nm which in accordance to reports of Ma et al. (2013) and Foroozandeh and Aziz (2018) is suitable for the cellular internalization of nanocomposite either by endocytosis or adsorption mechanism. As the particle size of FU@ZIF-L nanocomposite is less than 100 nm, it is suitable for biomedical applications. Zeta potential value of FU@ZIF-L was observed to be −1.74 mV (Fig. 4C). Negative charge prevents agglomeration of FU@ZIF-L nanocomposite promoting uniform dispersion of nanocomposite in the medium. In addition, FU@ZIF-L facilitates cellular uptake through non-specific interaction and adsorption by the few cationic sites in the cell membrane such as cationic cell penetrating peptide leading to the formation of clusters because of repulsive interaction with negatively charge domain in the cell surface. The adsorbed negatively charged particle undergoes localized neutralization and subsequent endocytosis leading to cellular intake (Wilhelm et al. 2003; Wang et al. 2008).

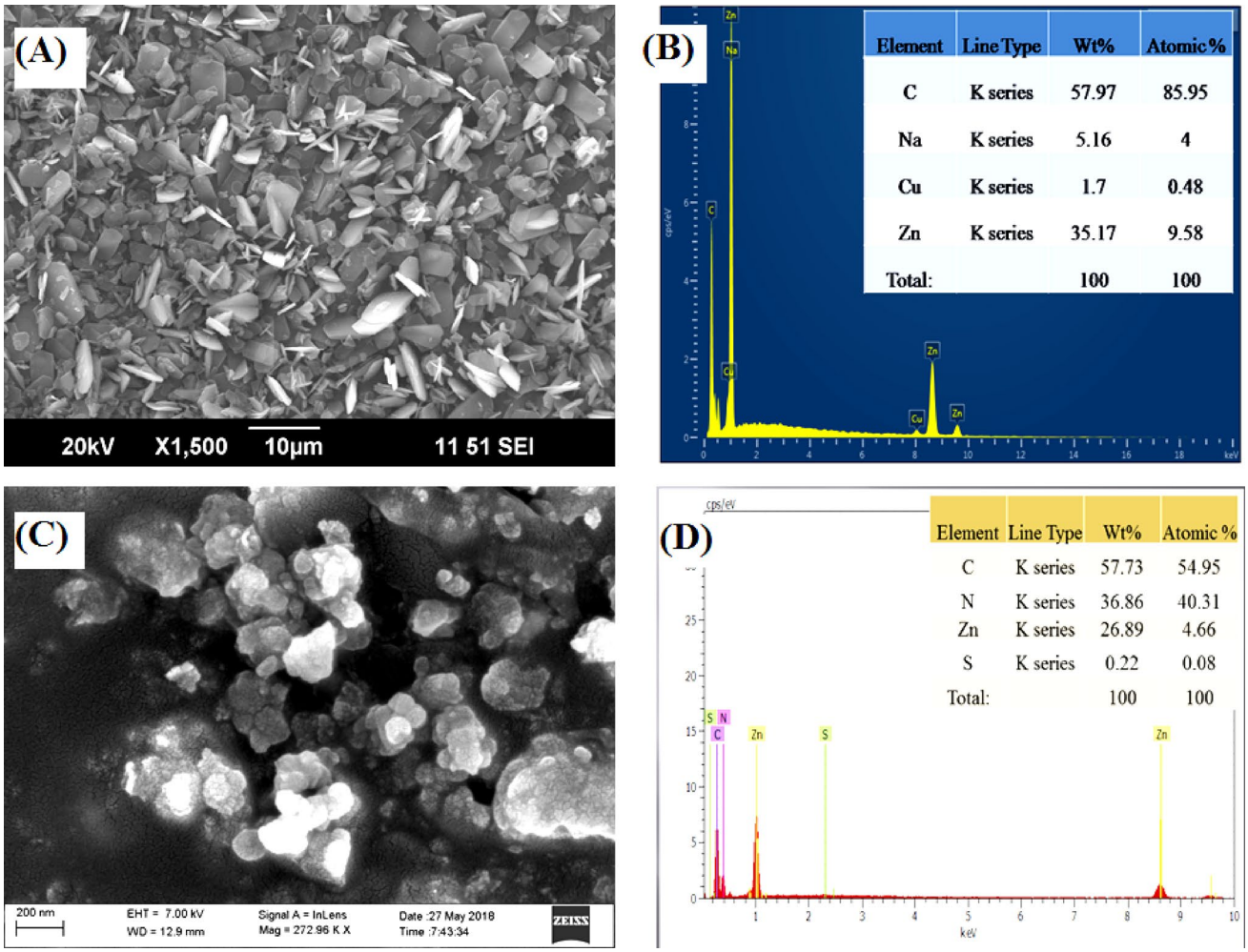

Fig. 3 SEM and EDX spectra of ZIF-L (**A**, **B**) and FU@ZIF-L(**C**, **D**)

Stimuli-based drug release mechanism of FU@ZIF-L nanocomposite

Stimuli-based drug delivery overcomes the drawback of classical drug delivery methods, by enhancing the programmed drug release on targeted site, hence pH-responsive drug release is considered as most reliable method for targeted drug delivery applications. The organic binder 2-methyl imidazole bonds get cleaved from ZIF-L at acidic conditions. Figure 5 shows gradual increase in the amount of fucoidan released under acidic pH 5 and 6, which reached the stationary phase at 36 and 39 h with no further drastic changes in drug release up to 48 h. However, at the physiological pH 7.4, a very slow drug release was observed with the passage of time (Fig. 5). At pH 7.4, the FU@ZIF-L nanocomposite was observed to be stable with a release capacity of 13.2%, however, when the pH was reduced to 5 and 6 (tumor cell micro-environment), the release capacity of the drug was relatively increased to 77 and 58% at the optimum time period of 36 and 39 h, respectively. The slow release at the physiological pH 7.4 illustrated that the hydro-stability and hydrophobic nature of ZIF-L might be responsible for the slow release of fucoidan, while enhanced drug release at acidic pH might be due to disintegration of ZIF-L structure, caused by the protonation of imidazole ring, leading to the break in the coordination bond between Zn and imidazole ions (Prabhu et al. 2019). Results of release kinetic studies revealed that, FU@ZIF-L nanocomposite is a promising material for pH-responsive drug delivery for cancer therapy.

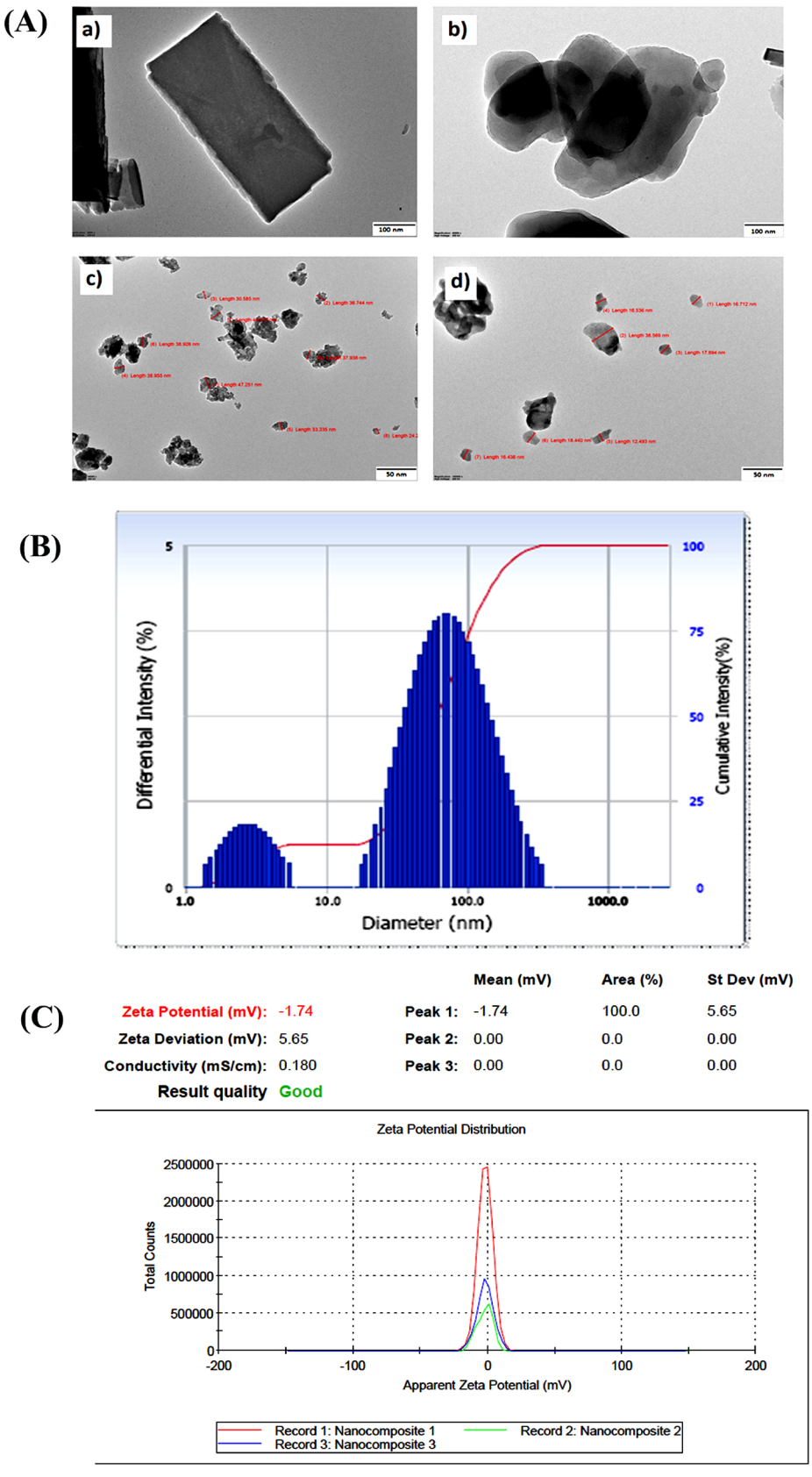

Fig. 4 **A** TEM images of ZIF-L (a, b) and FU@ZIF-L (c, d); **B** Particle size analysis of FU@ZIF-L by DLS; (C) Surface charge of FU@ZIF-L was analyzed using zeta potential analyzer

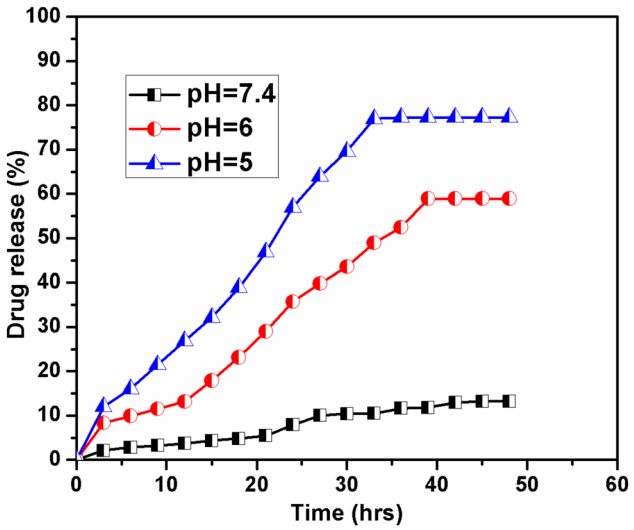

Fig. 5 Cumulative drug release of FU@ZIF-L nanocomposite at different pH (5, 6 and 7.4)

Anticancer potentialof FU@ZIF-L nanocomposite

Lung cancer is the deadliest form of cancer and leading causative of cancer related death with only 15% survivability for 5 years on incidence. Non-small cell lung carcinoma accounts for 85% of the total lung cancer cases. Current therapeutic strategies based on stage of diagnosis and type of malignancy involves surgery, combination of chemotherapy and radiation therapy and immunotherapy (Siegel et al. 2017). However, these treatment strategies suffer certain limitations such as low bioavailability due to poor solubility, toxic effect to healthy tissue due to non-specific drug deliver which turned the interest of researchers towards nanomaterials as cargo for efficient drug delivery. In this study, zeolitic imidazole frameworks (ZIF-L) acts as a carrier for fucoidan molecules, its deliver the drug molecules based on the pH-responsive mechanism. Anti-proliferative activity of free fucoidan, ZIF-L and FU@ZIF-L nanocomposite was evaluated by MTT assay against A549 cells. Results showed that ZIF-L exhibited very low cytotoxic effect even at highest concentration of 100 µg/ml. On the other hand, FU@ZIF-L nanocomposite and ZIF-L showed dose dependant increase in cytotoxicity with IC_{50} value of 38.5 ± 2.34 and 40 ± 1.24 µg/ml, respectively (Fig. 6A). FU@ZIF-L nanocomposite exhibits slightly higher cytotoxic effect of 89.02 ± 1.71% at the maximum concentration of 100 µg/ml on comparison with same dose of fucoidan alone revealing the fact that ZIF-L retains the cytotoxic effect of fucoidan after encapsulation. Morphological changes in the cells treated with FU@ZIF-L nanocomposite was evaluated by phase contrast microscopic analysis. Results revealed that (Fig. 6B) both FU@ZIF-L nanocomposite and fucoidan-treated cells exhibited cells with apoptotic characteristics such as membrane damage, shrinked cell with condensed chromatin and apoptotic body formation, while the control and ZIF-L-treated cells exhibited normal epithelial cells morphology. When compared to vehicle control, reduction in cell count was observed in ZIF-L-treated cells. FU@ZIF-L nanocomposite and fucoidan-treated cells showed drastic reduction in the cell number, when compared to control groups revealing its anti-proliferative and apoptotic effect.

Most of the chemotherapeutic agents cause cell death either by directly damaging nucleic acid or by disrupting the redox balance of cell and in both the cases ROS acts as key factor for apoptosis (Zaidieh et al. 2019). Based on this context, intracellular ROS level of FU@ZIF-L nanocomposite-treated cells was assessed using DCFDH-DA. Microscopic observation revealed that fucoidan and FU@ZIF-L-treated groups showed intense green fluorescence intensity when compared to ZIF-L and vehicle control (Fig. 7A). Spectrofluorimetric assay illustrated increase in fluorescence intensity by four fold in FU@ZIF-L nanocomposite-treated group in comparison with vehicle control and two fold increase when compared to fucoidan alone (Fig. 7B). Increased green fluorescent intensity in FU@ZIF-L nanocomposite and fucoidan-treated groups reveals the fact that fucoidan increases the intracellular ROS level. Enhanced fluorescence was observed in FU@ZIF-L nanocomposite-treated groups when compared to fucoidan alone which might be due to combinatorial effect of Zn^{2+}ions and fucoidan released at acidic pH of tumor environment (Zheng et al. 2017).

Changes in the nuclear morphology of A549 cells treated with FU@ZIF-L nanocomposite were evaluated by Hoechst 33342 staining. In vehicle control cells, intact cells with light blue spherical intact nuclei was observed, while FU@ZIF-L nanocomposite and fucoidan-treated cells (Fig. 8A) showed uniformly bright blue fluorescence indicating highly condensed, fragmented nuclei the characteristic feature of apoptosis. Figure 8B reveals the percentage of cells with normal and abnormal nuclei. FU@ZIF-L nanocomposite- and fucoidan-treated cells showed 75.66 ± 2.25 and 65 ± 3.22% of cells with abnormal nuclei, when compared to

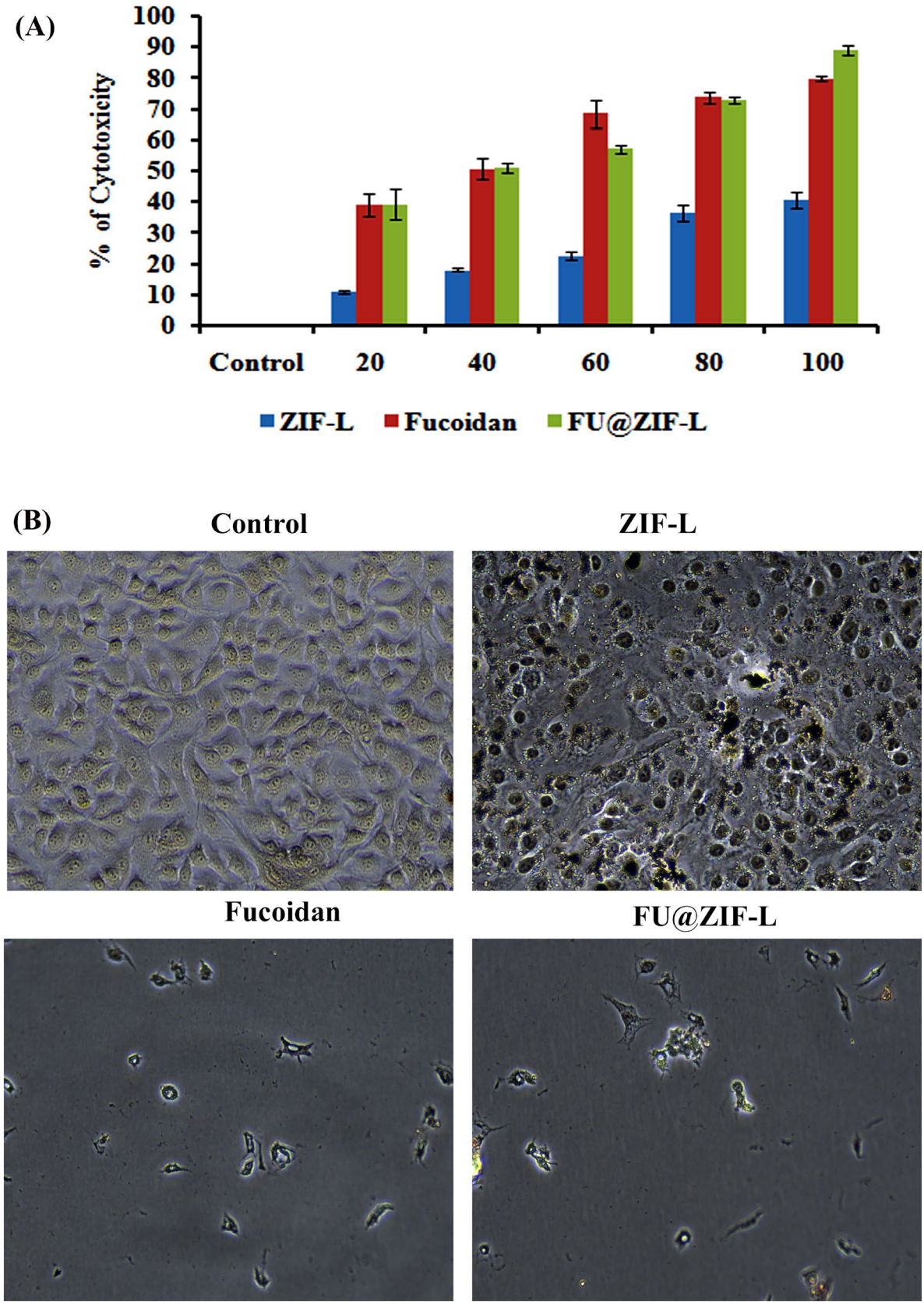

Fig. 6 **A** Assessment of cytotoxic effect of FU@ZIF-L in A549 cells by MTT assay; **B** Morphological assessment of treated A549 cells by phase contrast microscopic analysis (magnification 20×)

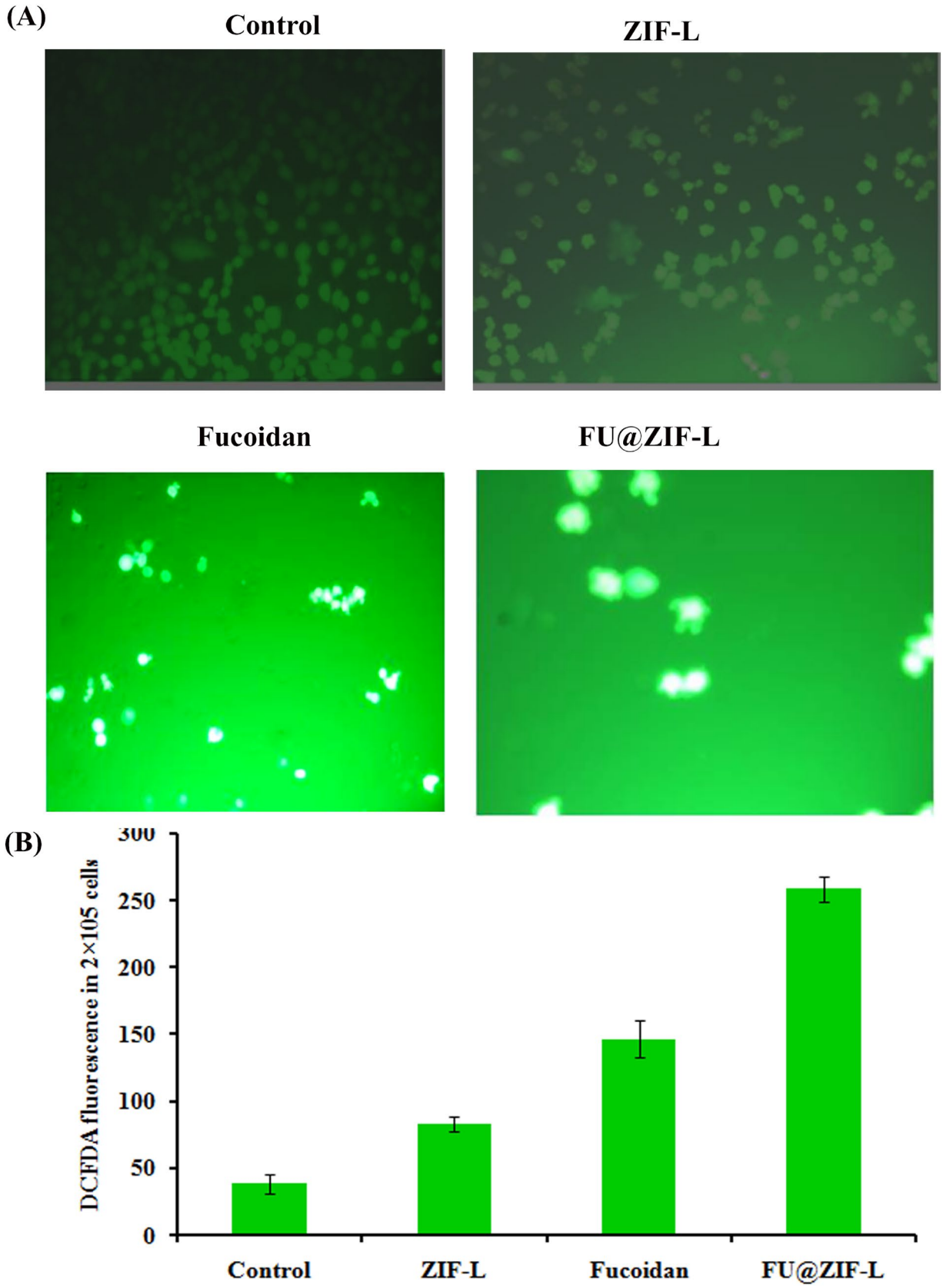

Fig. 7 **A** Fluorescence microscopic images of A549 cells after treatment of FU@ZIF-L illustrate intracellular ROS level (magnification 20×); **B** quantification of ROS level using fluorescence spectroscopy

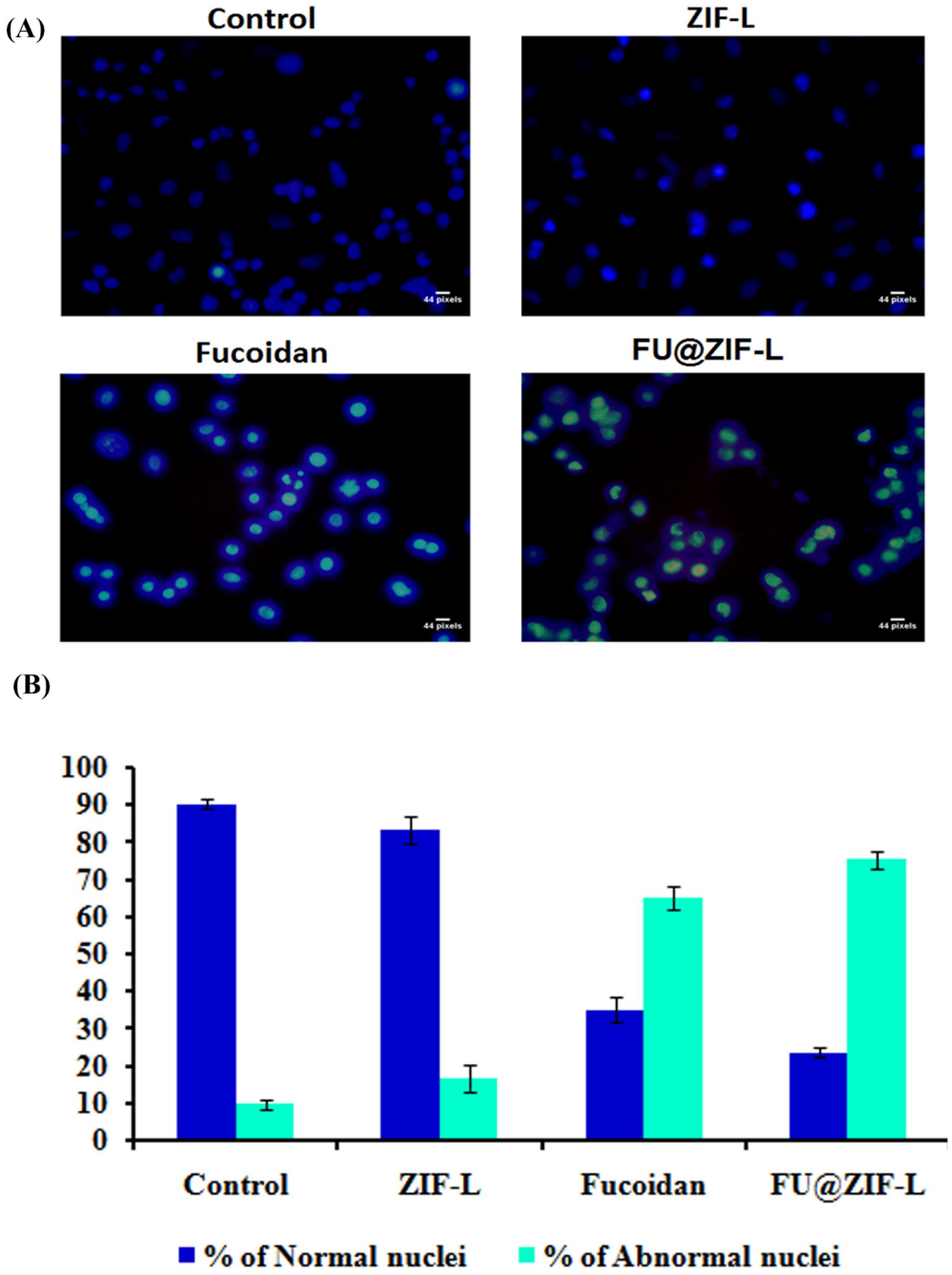

Fig. 8 A Assessment of changes in nuclear morphology of cells treated with FU@ZIF-L using Hoechst staining (magnification 20×); **B** quantitative evaluation of cells with normal and abnormal nuclei in control and treated groups

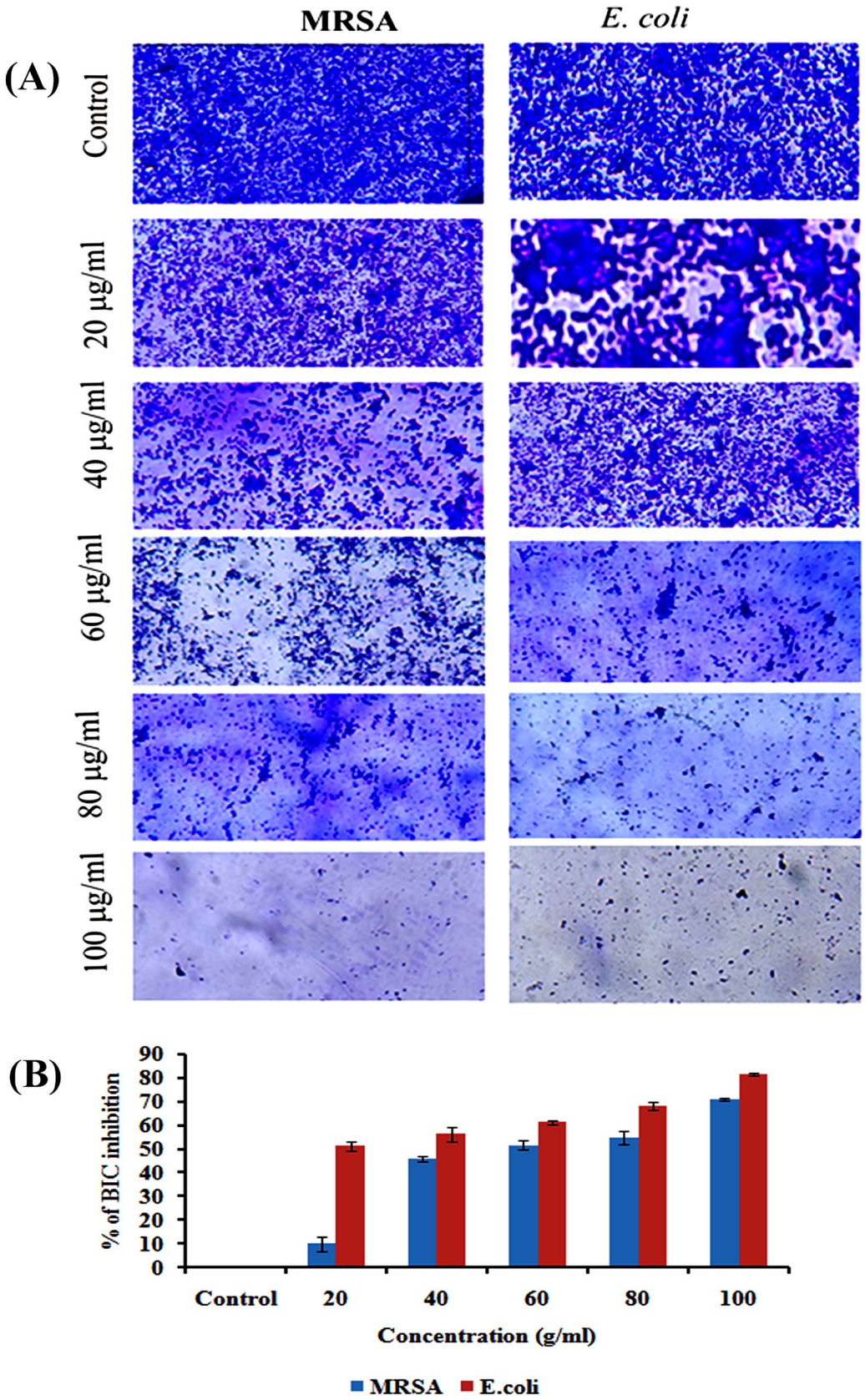

Fig. 9 **A** Light microscopic images revealing anti-biofilm activity of FU@ZIF-L in different doses (magnification 20×); **B** Quantification of anti-biofilm efficacy of FU@ZIF-L by crystal violet staining assay

Table 1 Antibacterial activity of FU@ZIF-L against clinical pathogens by agar well-diffusion method

Micro-organism	Positive control	Zone of inhibition (mm)		
		10 µg/ml	20 µg/ml	30 µg/ml
B. subtilis	12	10	14	18
S. aureus	14	15	16	20
K. pneumonia	14	12	16	21
E. coli	12	10	15	18

vehicle control and ZIF-L. Overall, the results revealed that FU@ZIF-L nanocomposite-treated cells showed enhanced ROS level provoking oxidative stress mediated mitochondrial dysfunction and nuclear damage ultimately leading to cell death. To conclude, anticancer efficiency of FU@ZIF-L nanocomposite might be due ROS-mediated activation of apoptotic pathway.

Anti-biofilm activity of FU@ZIF-L nanocomposite

Methicillin resistance *S. aureus* (MRSA) and *E. coli* are the two common opportunistic nosocomial pathogens, which creates serious problem in hospital environment. Besides being a major causative of recurrent urinary tract and skin infection *E. coli* and *MRSA* biofilms are responsible for in dwelling medical device related infectivity. Biofilm forming ability makes these bacterial species resistant to multidrug causing chronic life threatening infectious disease. In the present study, antibiofilm efficiency of FU@ZIF-L nanocomposite against MRSA and *E.coli* were analyzed and the results are depicted in Fig. 9A, B. Light microscopic observation of FU@ZIF-L nanocomposite-treated groups showed disruption in biofilm matrix of *E. coli* and *MRSA* with reduction in microcolonies, when compared to control which exhibited thick biofilm matrix (Fig. 9A). Results of crystal violet binding assay revealed that FU@ZIF-L nanocomposite showed decline in formation of biofilm in both MRSA and *E.coli* in concentration-dependent manner with highest inhibition of 70.82 ± 0.58 and $81.52 \pm 0.68\%$, respectively, at 100 µg/ml. IC_{50} value of FU@ZIF-L against MRSA and *E. coli* were observed to be 52.5 ± 1.05 and 19.29 ± 0.25 µg/ml, respectively. ZIF-L showed very less biofilm inhibitory activity, with no significant change in the biofilm architecture. Anti-biofilm activity of FU@ZIF-L nanocomposite might be due to biofilm inhibitory activity of fucoidan as

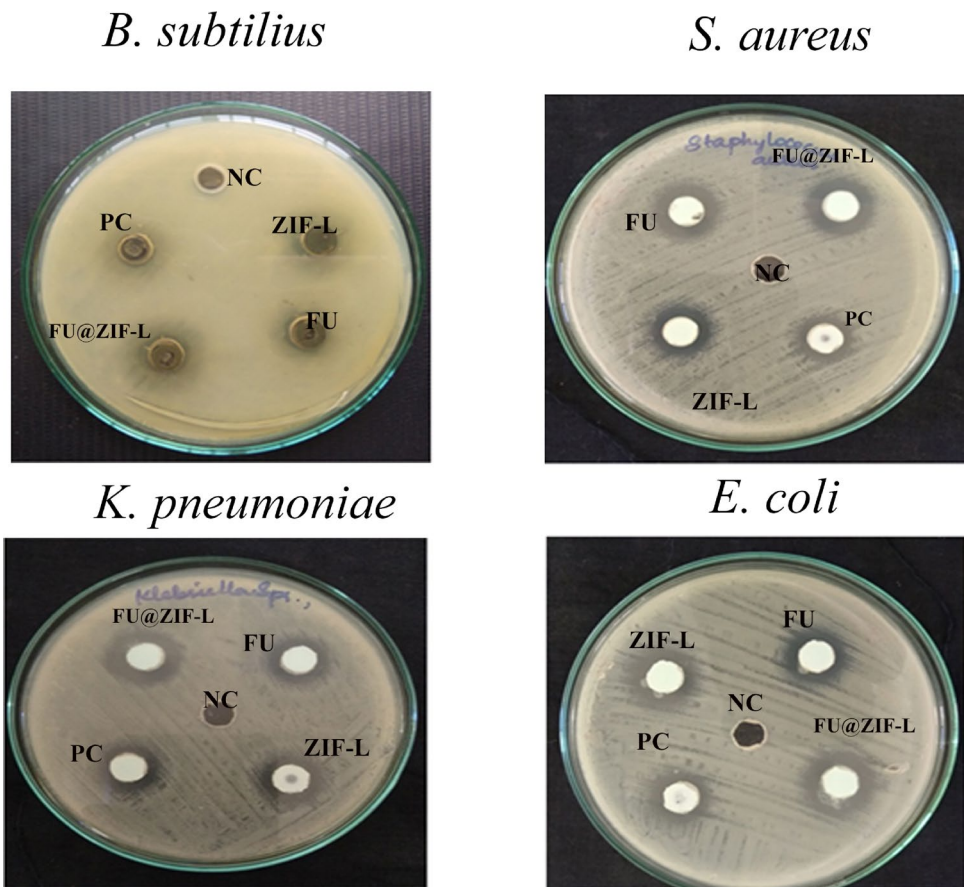

Fig. 10 Comparative analysis of antibacterial activity of FU@ZIF-L in comparison with bare ZIF-L and fucoidan

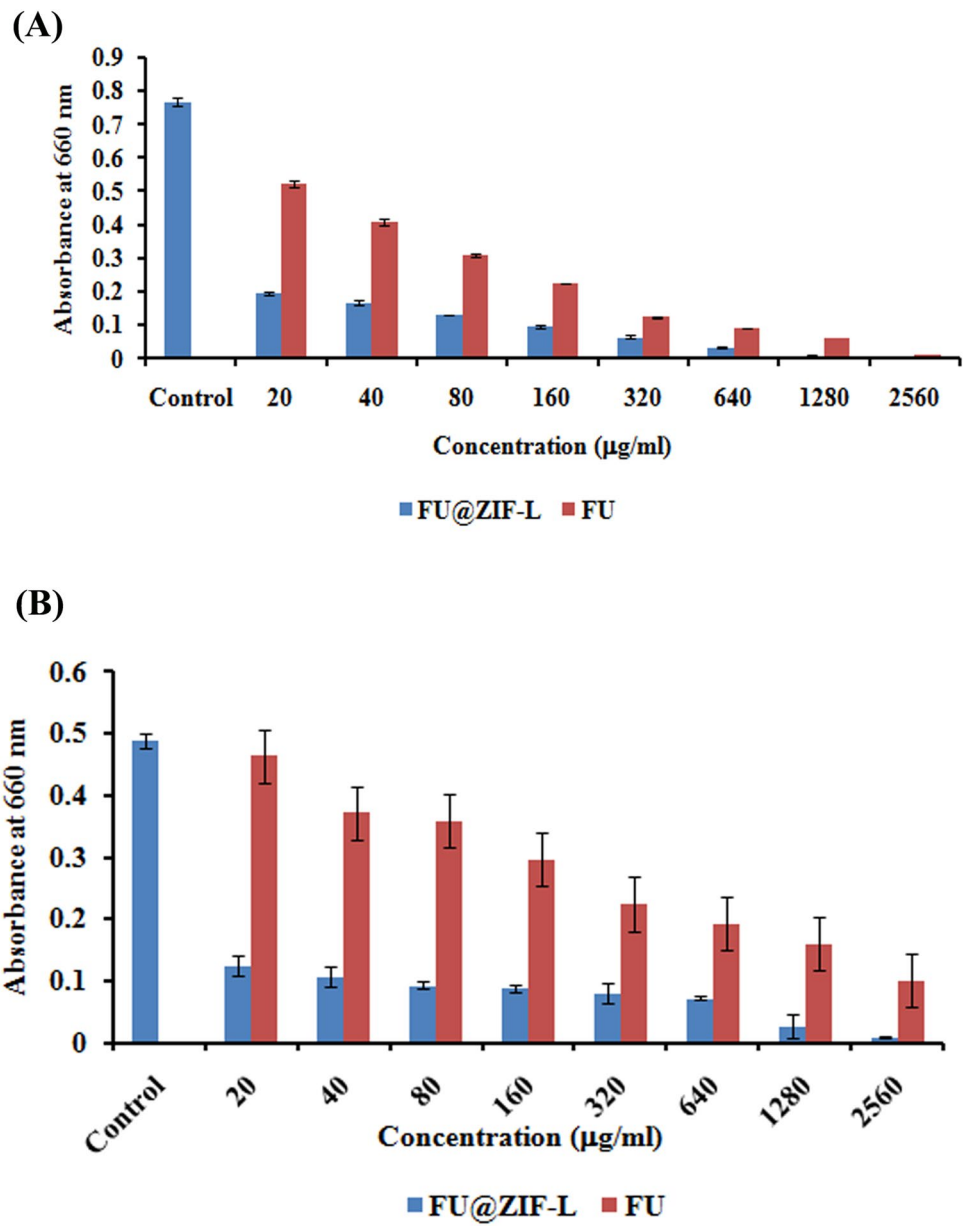

Fig. 11 Mininum inhibitory concentration (µg/ml) of FU@ZIF-L against **A** *S. aureus*; **B** *K. pneumonia*. Results are expressed as Mean ± S.D. of triplicate experiments

Table 2 Minimum bactericidal activity of FU@ZIF-L against *S. aureus* and *K. pneumonia*

Sample (concentration µg/ml)	CFU/ml	
	S. aureus	*K. pneumonia*
Control	TNTC	TNTC
20	TNTC	TNTC
40	TNTC	TNTC
80	TNTC	TNTC
160	TNTC	TNTC
320	1×10^2	2×10^2
640	50	120
1280	NIL	20
2560	NIL	NIL

per report of Jun et al. (2018). In addition, ZIF-L disintegrates at acidic pH environment induced by the formation of biofilm releasing Zn^{2+} which inhibits biofilm formation either by attenuating its swarming ability or by reducing the secretion of exo-polysaccharides as reported by Mahamunia et al. (2019). As biofilm matrix act as a diffusion barrier for antibiotic, creating a major challenge for antibiotic therapy, disruption of biofilm matrix by FU@ZIF-L nanocomposite, suggesting it as a suitable candidate for the prevention and inhibition of biofilm forming drug-resistant bacterial infection.

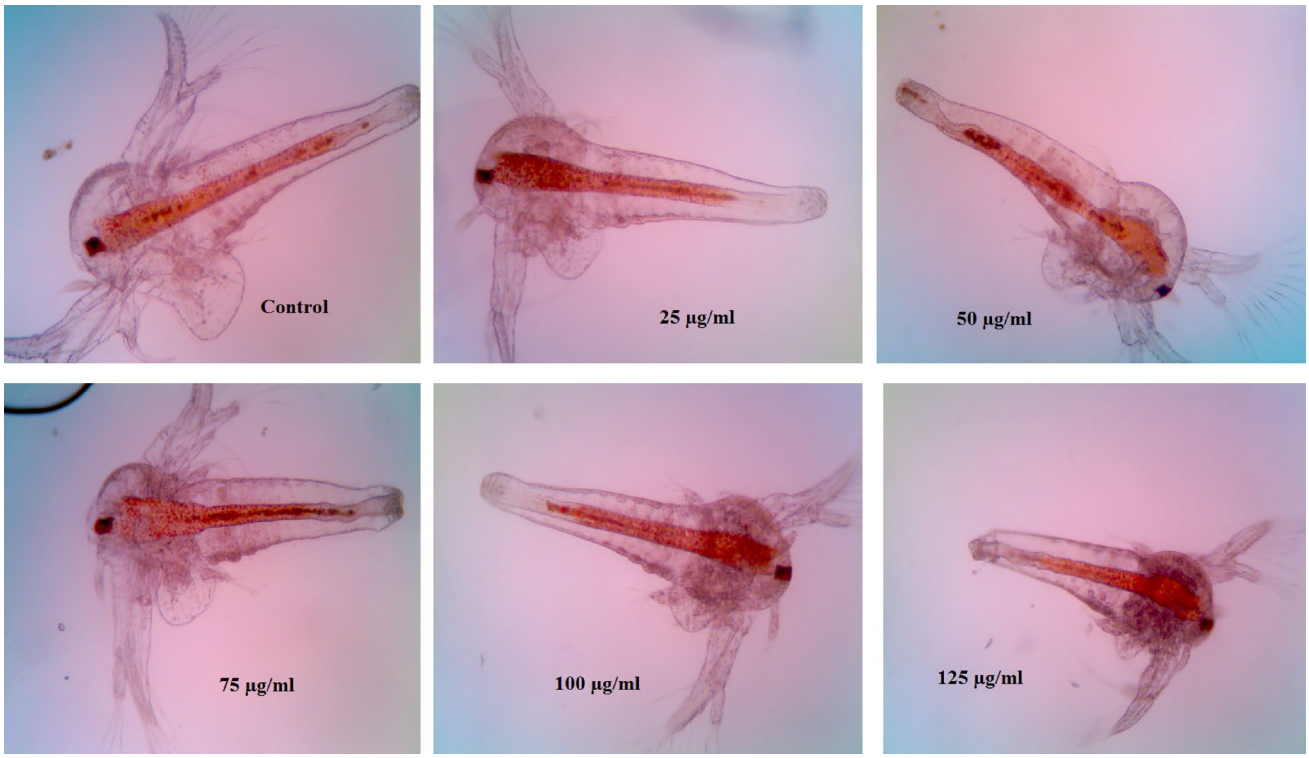

Fig. 12 Evaluation of morphological changes of *Artemia salina* nauplii post exposure to FU@ZIF-L nanocomposite (magnification 10×)

Antimicrobial activity of FU@ZIF-L nanocomposite

Antimicrobial efficiency of FU@ZIF-L nanocomposite against human pathogens was assessed by agar well-diffusion method. Results illustrate that FU@ZIF-L showed dose-dependent increase in antimicrobial activity against *B. subtilis, S. aureus, K. pneumonia* and *E. coli* with highest activity at 30 µg/ml (Table 1). Comparative analysis of antimicrobial activity of FU@ZIF-L nanocomposite and ZIF-L revealed that FU@ZIF-L nanocomposite exhibited highest growth inhibition against *B. subtilis, S. aureus, K. pneumonia* and *E. coli* with inhibition zone of 18 mm, 20 mm, 17 mm and 21 mm, respectively, when compared to fucoidan and ZIF-L alone (Fig. 10). MIC is the minimum concentration of FU@ZIF-L at which no visible growth of bacteria was observed in 24 h. Figure 11 illustrates reduction in bacterial cell viability significantly ($p < 0.05$), with an increase in concentration of FU@ZIF-L (20–2560 µg/ml) in both *S. aureus* and *K. pneumonia*. Bacteriostatic concentration of FU@ZIF-L for *S. aureus* and *K. pneumonia* was observed at 1280 µg/ml (Fig. 11A, B). Bacteriocidal concentration is the least dose of FU@ZIF-L essential for complete eradication of bacteria. For *S. aureus* and *K. pneumonia*, the MBC value was observed at 1280 and 2560 µg/ml of FU@ZIF-L (Table 2). Mechanism of antibacterial activity of FU@ZIF-L nanocomposite might be due to electrostatic force of interaction between the positively charged Zn^{2+}ions in ZIF-L and negatively charged lipopolysaccharide of bacterial cell wall altering integrity of phospholipid bilayer, facilitating its penetration into the bacterial cell. Zn^{2+} ions and fucoidan released intracellularly promoted ROS production-inducing apoptosis (Tong et al. 2013; Poveda Castillo et al. 2018).

Biocompatibility of FU@ZIF-L nanocomposite

Artemia salina is one of the most widely used test organism for ecotoxicology. Low cost, convenience and quick results of Artemia-based assay has turned the interest of researchers towards it as an alternative for assessing the toxicity of nanoparticles (Rajabiet al. 2015). In the present study, the biocompatibility of FU@ZIF-L nanocomposite was assessed by brine shrimp lethality bioassay. Results revealed that no noteworthy alteration in morphological features were seen in *Artemia salina* nauplii treated with FU@ZIF-L up to the dose of 75 µg/ml, while mortality was observed at the high dose of 125 µg/ml. The LC_{50} of FU@ZIF-Lnanocomposite was calculated to be as 108.43 ± 0.16 µg/ml (Fig. 12). Swimming behavior of FU@ZIF-L-treated groups were observed to be normal at the end of 48 h illustrating the fact that FU@ZIF-L nanocomposite is non-toxic at low doses with mild toxicity at the higher concentration. Results reveal that FU@ZIF-L nanocomposite is biocompatible in nature and can act as a suitable drug delivery system.

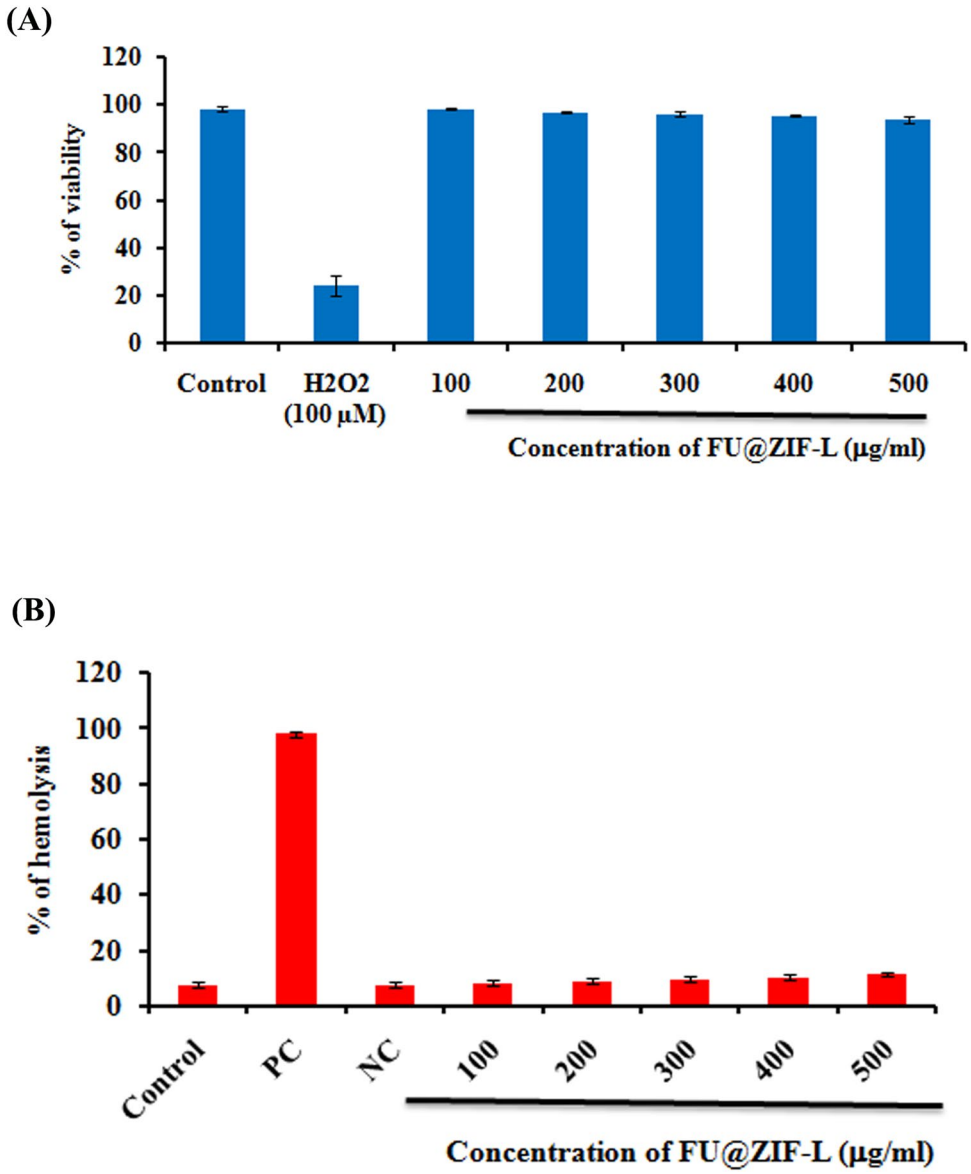

Fig. 13 **A** Cytotoxic effect of FU@ZIF-L nanocomposite (100–500 µg/ml) on PBMC in comparison with 250 µM H_2O2 at 24 h; **B** In vitro hemolytic effect of FU@ZIF-L nanocomposite (100–500 µg/ml) on human erythrocyte. Results are expressed as the Mean ± SD ($n = 3$)

Safety evaluation of FU@ZIF-L under in vitro condition

Nanomaterials used for biomedical applications should be biocompatible in nature; hence, assessment of safety aspects of prepared nanomaterial is essential prior to its applications (Wolfram et al. 2015). In vitro cytotoxic effect of FU@ZIF-L was assessed using human peripheral mononuclear cells as model system which were widely used for preliminary toxicity studies prior to preclinical studies (Kandárová et al. 2011; Pourahmad and Salimi 2015). Trypan blue exclusion assay was used to evalulate the in vitro cytotoxic effects of FU@ZIF-L. Results revealed that FU@ZIF-L at its maximum dose (500 µg/ml) showed no noteworthy alteration in cell membrane integrity at the and the percentage of cell viability was observed to be 93.66 ± 1.3% similar to vehicle control (Fig. 13A). Positive control-treated cells exhibited cell viability of 24.09 ± 0.49% revealing the non-cytotoxic nature of FU@ZIF-L.

Hemolytic activity was used to analyze the compatibility of nanomaterials with blood cells (Zohra and Fawzia 2014). FU@ZIF-L showed mild hemolytic activity in concentration dependant manner with 11.33 ± 0.5% hemolytic activity at the optimum dose (500 µg/ml). Positive control (Triton X-100, 0.2%)-treated cells showed 98 ± 0.89% hemolysis, while buffer-treated RBC showed 7.66 ± 0.5% hemolysis (Fig. 13B). Results reveal that FU@ZIF-L is non hemolytic in nature based on the report of Ralph et al. (1998) indicating the fact that FU@ZIF-L nanocomposite induced no major detectable disturbance in the RBC membrane. Overall, the results of in vitro toxicity studies reveal that FU@ZIF-L nanocomposite is neither cytotoxic to PBMC and

nor hemolytic to RBC indicating its biocompatible nature to human blood cells.

Conclusion

The present study reports successful fabrication of FU@ZIF-L nanocomposite by eco-friendly method. Fabricated FU@ZIF-L nanocomposite showed high drug (fucoidan) loading efficiency and synergistic effects in anticancer studies. FU@ZIF-L nanocomposite exhibited potent bactericidal activity against dreadful human pathogens. In addition, FU@ZIF-L nanocomposite disrupts the biofilm matrix of MRSA and *E. coli*, which indicates that, FU@ZIF-L nanocomposite acts as a suitable candidate in eradicating multidrug-resistant bacteria. FU@ZIF-L nanocomposite exhibits its anticancer potential via ROS-induced nuclear damage leading to apoptosis in lung cancer cells. Safety evaluation studies revealed that FU@ZIF-L exhibited neither cytotoxic effect nor hemolytic effect. Brine shrimp lethality assay confirms the biocompatible nature of FU@ZIF-L nanocomposite. Overall findings of the present study revealed that FU@ZIF-L nanocomposite acts as an effective material for biomedical applications.

Acknowledgements R. Prabhu and N. Suganthy thank RUSA-Phase 2.0 Grant (No. F. 24-51/2014-U, Policy (TN Multi-Gen), Dept. of Edn. Govt.of India, (Dated: 09.10.2018). Authors also acknowledge the Department of Science and Technology, New Delhi for the financial support in general and infrastructure facilities sponsored under PURSE 2nd Phase programme (Order No. SR/PURSE Phase 2/38 (G) dated: 21.02.2017).

Declarations

Conflict of interest On behalf of the authors declared that there is no conflict of interest.

References

Abdelhamid HN, Huang Z, El-Zohry AM, Zheng H, Zou X (2017) A fast and scalable approach for synthesis of hierarchical porous zeolitic imidazolate frameworks and one-pot encapsulation of target molecules. ACS Inorg Chem 56(15):9139–9146

Adhikari C, Das A, Chakraborty A (2015) Zeolitic imidazole framework (ZIF) nanospheres for easy encapsulation and controlled release of an anticancer drug doxorubicin under different external stimuli: a way toward smart drug delivery system. Mol Pharm 12(9):3158–3166

Ashayerizadeh O, Dastar B, Pourashouri P (2020) Study of antioxidant and antibacterial activities of depolymerized fucoidans extracted from Sargassum tenerrimum. Int J Biol Macromol 151:1259–1266

Biswal BP, Shinde DB, Pillai VK, Banerjee R (2013) Stabilization of graphene quantum dots (GQDs) by encapsulation inside zeolitic imidazolate framework nanocrystals for photoluminescence tuning. RSC Nanoscale 5(21):10556–10561

Chen R, Yao J, Gu Q, Smeets S, Baerlocher C, Gu H, Zhu D, Morris W, Yaghi O, Wang H (2013) A two-dimensional zeoliticimidazolate framework with a cushion-shaped cavity for CO2 adsorption. Chem Commun 49:9500–9502

Cho Y, Yoon JH, Yoo JJ, Lee M et al (2015) Fucoidan protects hepatocytes from apoptosis and inhibits invasion of hepatocellular carcinoma by up-regulating p42/44 MAPK-dependent NDRG-1/CAP43. Acta Pharm Sin B 5:544–553

Chowdhuri AR, Laha D, Pal S, Karmakar P, Sahu SK (2016) One-pot synthesis of folic acid encapsulated upconversionnanoscalemetalorganic frameworks for targeting, imaging and pH responsive drug release. Dalton Trans 45(45):18120–18132

CLSI (2006) Performance standards for antimicrobial disk susceptibility tests. Approved standard 9th ed. Document M2-A9, Clinical and Laboratory Standards Institute, Wayne, PA.

Deepika MS, Thangam R, Sheena TS, Sasirekha R et al (2019) A novel rutin-fucoidan complex based phytotherapy for cervical cancer through achieving enhanced bioavailability and cancer cell apoptosis. Biomed Pharmacother 109:1181–1195

Dobrovolskaia MA, Clogston JD, Neun BW, Hall JB, Patri AK, McNeil SE (2008) Method for analysis of nanoparticle hemolytic properties in vitro. Nano Lett 8(8):2180–2187

Foroozandeh P, Aziz AA (2018) Insight into cellular uptake and intracellular trafficking of nanoparticles. Nanoscale Res Lett 13:339. https://doi.org/10.1186/s11671-018-2728-6

He M, Zhou J, Chen J, Zheng F, Wang D, Shi R, Guo Z, Wang H, Chen Q (2015) Fe 3 O 4@ carbon@ zeolitic imidazolate framework-8 nanoparticles as multifunctional pH-responsive drug delivery vehicles for tumor therapy in vivo. J Mater Chem B3(46):9033–9042

Ikeguchi K, Saito H, Miki Y, Kimura T (2015) Effect of fucoidan dietary supplement on the chemotherapy treatment of patients with unresectable advanced gastric cancer. J Cancer Ther 6:1020–1026

Ishwarya R, Vaseeharan B, Kalyani S et al (2018) Facile green synthesis of zinc oxide nanoparticles using Ulva lactuca seaweed extract and evaluation of their photocatalytic, antibiofilm and insecticidal activity. J Photochem Photobiol B 178:249–258

James JB, Lin YS (2016) Kinetics of ZIF-8 thermal decomposition in inert oxidizing, and reducing environments. J Phys Chem C 120(26):14015–14026

Jun JY, Jung MJ, Jeong IH, Yamazaki K, Kawai Y, Kim BM (2018) Antimicrobial and anti-biofilm activities of sulfated polysaccharides from marine algae against dental plaque bacteria. Mar Drugs 16(9):301. https://doi.org/10.3390/md16090301

Kambe T, Tsuji T, Hashimoto A, Itsumura N (2015) The physiological, biochemical, and molecular roles of zinc transporters in zinc homeostasis and metabolism. Physiol Rev 95:749–784

Kandárová H, Letašiová S (2011) Alternative methods in toxicology: pre-validated and validated methods. Interdiscip Toxicol 4(3):107–113

Khan F, Manivasagan P, Won Lee J, Nguyen Pham DT, Oh J, Kim YM (2019) Fucoidan stabilized gold nanoparticle mediated biofilm inhibition, attenuation of virulence and motility properties in *Pseudomonas aeruginosa* PAO1. Mar Drugs 17(4):208. https://doi.org/10.3390/md17040208

Khana IU, Dzarfan Othman MH, Ismaila AF, IsmailaN JJ, Hashima H, Rahmana MA, Jilania A (2018) Structural transition from two-dimensional ZIF-L to three-dimensional ZIF-8 nanoparticles in

aqueous room temperature synthesis with improved CO2 adsorption. Mater Charact 136:407–416
Lee WC, Chien HT, Lo Y, Chiu HC, Wang TP, Kang TY (2015) Synthesis of zeolitic imidazolate framework core–shell nanosheets using zinc-imidazole pseudopolymorphs. ACS Appl Mater Interfaces 7(33):18353–18361
Li J, Chen K, LiS FJ, Liu T, Wang F, Zhang R et al (2016) Protective effect of fucoidan from Fucusvesiculosus on liver fibrosis via the TGF-beta1/Smad pathway-mediated inhibition of extracellular matrix and autophagy. Drug Des Dev Ther 10:619–630
Ma N, Ma C, Li C, Hel N (2013) Influence of nanoparticle shape, size, and surface functionalization on cellular uptake. J Nanosci Nanotechnol 13(10):6485–6498
Mahamunia PP, Patila PM, Dhanavadeb MJ, Badigerc MV, Shadijaa PG, Lokhanded AC, Bohara RA (2019) Synthesis and characterization of zinc oxide nanoparticles by using polyol chemistry for their antimicrobial and anti-biofilm activity. Biochem Biophys Rep 17:71–80
McNamara K, Tofail SAM (2017) Nanoparticles in biomedical applications. Adv Phys X 2(1):54–88
Narasimhan B, Sharma D, Kumar P (2011) Biological importance of imidazole nucleus in the new millennium. Med Chem Res 20:1119–1140
Pourahmad J, Salimi A (2015) Isolated human peripheral blood mononuclear cell (PBMC), a cost effective tool for predicting immunosuppressive effects of drugs and xenobiotics. Iran J Pharm Res 14(4):979
Poveda Castillo GDC, Rodrigo D, Martínez A, Pina Pérez MC (2018) Bioactivity of fucoidan as an antimicrobial agent in a new functional beverage. Beverages 4(3):64. https://doi.org/10.3390/beverages4030064
Prabhu R, Mohamed AR, Anjali R, Archunan G, Prabhu NM, Pugazhendhi A, Suganthy N (2019) Ecofriendly one pot fabrication of methyl gallate@ZIF-L nanoscale hybrid as pH responsive drug delivery system for lung cancer therapy. Process Biochem 84:39–52
Prabhu R, Pugazhendhi A, Suganthy N (2020) One-pot fabrication of multifunctional catechin@ZIF L nanocomposite: assessment of antibiofilm, larvicidal and photocatalytic activities. J Photochem Photobiol B 203:111774. https://doi.org/10.1016/j.jphotobiol.2019.111774
Rajabi S, Ramazani A, Hamidi M, Naji T (2015) Artemia salina as a model organism in toxicity assessment of nanoparticles. Daru J Pharm Sci 23(1):20. https://doi.org/10.1186/s40199-015-0105-x
Ralph ET, Guest JR, Green J (1998) Altering the anaerobic transcription factor FNR confers a hemolytic phenotype on *Escherichia coli* K12. Proc Natl Acad Sci USA 95:10449–10452
Shanholtzer CJ, Peterson LR, Mohn ML, Moody JA, Gerding DN (1984) MBCs for *Staphylococcus aureus* as determined by macrodilution and microdilution techniques. Antimicrob Agents Chemother 26(2):214–219
Siegel RL, Miller KD, Fedewa SA, Ahnen DJ, Meester RGS, Barzi A, Jemal A (2017) Evaluation of colorectal cancer statistics. CA: Cancer J Clin 67:177–193
Sivamaruthi B, Sri Ramkumar V, Archunan G, Chaiyasut C, Suganthy N (2019) Biogenic synthesis of silver palladium bimetallic nanoparticles from fruit extract of *Terminalia chebula*—in vitro evaluation of anticancer and antimicrobial activity. JDDST 51:139–150
Sun CY, Qin C, Wang XL, Yang GS, Shao KZ, Lan YQ, Su ZM, Huang P, Wang CG, Wang EB (2012) Zeolitic imidazolate framework-8 as efficient pH-sensitive drug delivery vehicle. Dalton Trans 41(23):6906–6909
Tiwari A, Singh A, Garg N, Randhawa JK (2017) Curcumin encapsulated zeolitic imidazolate frameworks as stimuli responsive drug delivery system and their interaction with biomimetic environment. Sci Rep 7(1):12598. https://doi.org/10.1038/s41598-017-12786-6
Tong GX, Du FF, Liang Y, HuQ Wu, RN, Guan, JG, Hu X, (2013) Polymorphous ZnO complex architectures: selective synthesis, mechanism, surface area and Zn-polar plane-codetermining antibacterial activity. J Mater Chem B 1(4):454–463
Wang B, Zhang L, Bae SG, Granick S (2008) Nanoparticle induced surface reconstruction of phospholipid membranes. Proc Matl Acad Sci Unit States Am 105(47):18171–18175
Wang XG, Dong ZY, Cheng H, Wan SS et al (2015) A multifunctional metal-organic framework based tumortargeting drug delivery system for cancer therapy. RSC Nanoscale 7(38):16061–16070
Wilhelm C, Billotey C, Joger J, Pons JN, Baeri JC, Gazeau F (2003) Intracellular uptake of anionic superparamanetic nanoparticles as a function of their coating. Biomaterials 24:1001–1011
Wolfram J, Zhu M, Yang Y et al (2015) Safety of nanoparticles in medicine. Curr Drug Targets 16(14):1671–1681
Yu H, Qiu X, Neelakanda P, Deng L, Khashab NM, Nunes SP, Peinemann KV (2015) Hollow ZIF-8 nanoworms from block copolymer templates. Sci Rep 5:15275. https://doi.org/10.1038/srep15275
Zaidieh T, Smith JR, Ball KE et al (2019) ROS as a novel indicator to predict anticancer drug efficacy. BMC Cancer 19:1224. https://doi.org/10.1186/s12885-019-6438-y
Zhang SM, Xie ZP, Xu L, Shi LF (2015) Cardioprotective effects of fucoidan against hypoxia-induced apoptosis in H9c2 cardio myoblast cells. Pharm Biol 53:1352–1357
Zhang FM, Dong H, Zhang X, Sun XJ, Liu M, Yang DD, Liu X, Wei JZ (2017) Postsynthetic modification of ZIF-90 for potential targeted codelivery of two anticancer drugs. ACS Appl Mater Interfaces 9(32):27332–27337
Zheng H, Zhang Y, Liu L, Wan W, Guo P, Nyström AM, Zou X (2016) One-pot synthesis of metal–organic frameworks with encapsulated target molecules and their applications for controlled drug delivery. J Am Chem Soc 138(3):962–968
Zheng C, Wang Y, Fiona Phua SZ, Lim WQ, Zhao Y (2017) ZnO–DOX@ZIF-8 core-shell nanoparticles for pH responsive drug delivery. ACS Biomater Sci Eng 3(10):2223–2229